npj | Computational Materials

www.nature.com/npjcompumats

ARTICLE OPEN

Insight into point defects and impurities in titanium from first principles

Sanjeev K. Nayak[1], Cain J. Hung[1], Vinit Sharma[1,5], S. Pamir Alpay[1,2], Avinash M. Dongare[1], William J. Brindley[3] and Rainer J. Hebert[1,4]

Titanium alloys find extensive use in the aerospace and biomedical industries due to a unique combination of strength, density, and corrosion resistance. Decades of mostly experimental research has led to a large body of knowledge of the processing-microstructure-properties linkages. But much of the existing understanding of point defects that play a significant role in the mechanical properties of titanium is based on semi-empirical rules. In this work, we present the results of a detailed self-consistent first-principles study that was developed to determine formation energies of intrinsic point defects including vacancies, self-interstitials, and extrinsic point defects, such as, interstitial and substitutional impurities/dopants. We find that most elements, regardless of size, prefer substitutional positions, but highly electronegative elements, such as C, N, O, F, S, and Cl, some of which are common impurities in Ti, occupy interstitial positions.

npj Computational Materials (2018)4:11 ; doi:10.1038/s41524-018-0068-9

INTRODUCTION

Point defects play a key role in mechanical properties of metallic materials and in diffusive phase transformations.[1] Commonly considered point defects are interstitials, including self-interstitials, substitutional atoms, and vacancies.[2] The most important extrinsic elements for point defects in titanium and its alloys are nitrogen, hydrogen, oxygen, and carbon. Oxygen plays a special role due to a large chemical affinity with titanium and a substantial solubility in both hexagonal close packed (hcp) and body centered cubic (bcc) titanium. The large solubility of oxygen, nitrogen, and hydrogen in titanium was mentioned by Fast as early as 1938.[3] Ehrlich was the first to examine the solubility of oxygen in titanium quantitatively and determined a solubility limit of 42 wt% oxygen in titanium. Ehrlich also observed a change in the *c/a* ratio of the hcp titanium lattice with oxygen increase. For pure titanium, the *c/a* ratio is less than the ideal value of 1.633; but it approaches 1.633 at higher oxygen contents. The thermodynamic assessment of the Ti–O system has in the meantime confirmed the limit to about 33 at% over a broad temperature range for Ti–O.[4] Interstitial elements in the hcp crystal structure produce non-symmetrical strain fields and are, therefore, effective in interacting with dislocations.[5] The resulting strengthening effect is exploited in commercially pure titanium alloys of grades 1–4 as the main strengthening mechanism and the yield strength increases with oxygen content as does the fatigue strength. For example, the yield strength of high-purity titanium (99.99 %) increases from about 322 MPa for low iron commercially pure titanium to about 420 MPa with an increase in oxygen content from 2100 ppm to 2900 ppm.[6] Eventually, at oxygen levels of about 0.25% the ductility and toughness decreases rapidly to the point where the titanium-oxygen alloy loses its structural materials capabilities. Hydrogen, while limited in solubility to about 1% at room temperature, diffuses orders of magnitude faster than other interstitial elements and readily forms hydrides that negatively impact mechanical properties.[7] Nitrogen has been shown to have the strongest strengthening effect per unit addition.[8] Interstitials in titanium form solid solutions, but at compositions exceeding the solid solution solubility limits can form compound phases. These compound phases are a problem in particular for hydrogen in titanium because of their brittle nature and vastly different elastic properties from the titanium matrix. The solubility of hydrogen in titanium at room temperature is thought to be between 20 and 200 ppm and increases with temperature to over 6000 ppm, but decreases with the presence of oxygen. The face centered cubic (fcc) hydride (δ) phase forms at hydrogen concentrations of more than 200 ppm in alpha-titanium.[9] But hydrogen also interacts with dislocations and cracks and has been shown to affect mechanical properties even at levels of less than 125 ppm.[10]

Interstitial impurities have long been recognized in melting practices and ingot production of titanium as sources for melt defects. Low-density inclusions (LDIs) are regions of interstitially-strengthened alpha phase with increased hardness, reduced ductility, and increased beta-transus temperature.[11] Strict processing controls have been implemented over the years for castings and forgings that have greatly reduced the occurrence of interstitial defects. In case of LDIs, for example, less than one defect is nowadays allowed per 500,000 kg of titanium alloy produced.[12] New technologies were introduced such as cold-hearth melting that contributed to the decrease in defect occurrence. But the ability to control impurity-related defects in titanium alloys has changed dramatically with the emergence of additive manufacturing. No longer is the processing limited to highly experienced titanium producers with unique

[1]Department of Materials Science and Engineering and Institute of Materials Science, University of Connecticut, Storrs, CT 06269, USA; [2]Department of Physics, University of Connecticut, Storrs, CT 06269, USA; [3]Pratt & Whitney, East Hartford, CT 06108, USA and [4]Additive Manufacturing Innovation Center, University of Connecticut, Storrs, CT 06269, USA

Correspondence: Sanjeev K. Nayak (sanjeev.nayak@uconn.edu) or Rainer J. Hebert (rainer.hebert@uconn.edu)

[5]Present address: Materials Science and Technology Division, Oak Ridge National Laboratory, Oak Ridge, TN 37831, USA

Received: 1 June 2017 Revised: 14 February 2018 Accepted: 14 February 2018
Published online: 16 March 2018

manufacturing technologies and environments such as vacuum-arc re-melting or cold-hearth melting furnaces. Instead, titanium components are manufactured from powder in additive manufacturing machines where the powder handling and storage and the environmental control in the machines is largely relegated to the users—opening up a wide range of processing practices and hence widely varying impurity levels. Worse, the multifold increase in specific surface area of powders over bulk materials exposes titanium and its alloys to interstitial elements in the atmosphere of the additive machines, notably oxygen, nitrogen and hydrogen. During electron-beam melting of titanium, the powder bed is kept at elevated temperatures during the build process and these elevated temperatures enhance impurity solubilities and diffusivities. Additive manufacturing practitioners would benefit from a deeper understanding of interactions in the metallic powder, particularly the effect of the machine environment (partial pressure of oxygen) and the role of impurities in changing the properties of powder. In order to decide on processing conditions, additive manufacturing practitioners might use these science-based guidelines for powder storage, handling, recycling, and the selection and control of build chamber atmospheres.

These science-based guidelines should start with the energetics of interstitials and vacancies at specific lattice sites and their distribution within the titanium host lattice and continue with the same considerations for substitutional elements. Density functional theory (DFT) calculations are well suited to determine the energies of interstitial atoms, vacancies, and substitutional atoms. There have been extensive DFT studies on titanium, notably, the role of point defects in $\alpha \leftrightarrow \omega$ structural transformation[13–15] and oxygen diffusion in the lattice,[16,17] generalized staking faults, such as, $(10\bar{1}2)$ twin boundaries and $(10\bar{1}0)$ prism plane stacking fault,[18] vacancy migration, first-principles thermodynamics based on cluster expansion formalism and Monte Carlo simulation, and in identifying the short range order.[19,20] Although there have been some efforts to systematically characterize the impurities in Ti, the problem has been mostly confined to defect complexes formed due to substitutional solutes and interstitial oxygen.[17] To this end, a systematic study on the role of various impurities in hcp titanium is highly desirable.

The topic of point defects has been studied using electronic structure methods since the early 1960s to explain the mechanism of self-diffusion in Cu and vacancy generation and migration in Cu.[21,22] The magnitude and the degree of anisotropy of the dielectric polarizability calculated for Al, Cu, and Mo provide clue that the <100> split configuration is prevalent in fcc metals while the <110> split configuration is prevalent in bcc metals.[23] Recently, there have been DFT models to study solute-vacancy interactions in Al, where the 3d series of elemental solutes were considered.[24] The ground state and thermodynamics of M-H systems (M = Al, Ba, Ca, K, Mg, La, Li, Na, Ni, Pd, Sc, Sr, Ti, V, and Y)[25] are also studied. H in Al and intermetallic precipitates Al–Cu–Mg–(Si) and Al–Zn–Mg commonly appear in the literature of Al alloys.[26] There has also been successful modeling of binary phase diagrams of Ti-transition metal alloys from first-principles methodologies.[27,28] Using molecular statics and dynamics study of stress effects on self-interstitial diffusion in Ti, it is pointed that uniaxial stress along the $[11\bar{2}0]$ direction could increase the growth rate of irradiation-induced voids by almost 20%.[29] Applying the continuum theory model, Šob et al. argue that the strengthening of hcp Ti by interstitial solutes (O, N, and C) is explained through a sessile-glissile dislocation transformation mechanism.[30] It is normally expected that metals with the same valence show similar plastic behavior. However, it was shown by an in situ transmission electron microscopy strain study and first-principles calculations that Ti and Zr, have the same valence, yet have different plasticity behavior due to the inversion of stability between the glissile and sessile dislocation cores.[31] Yu et al. have reported their study from first-principles theory that the profound hardening of hcp Ti by O impurities is due to the strong chemical interaction of O with the core of the dislocation.[16]

These results underline the important role of chemical hybridization in components of the alloy. In the present report, a systematic study of point defects in hcp Ti is undertaken using first-principles density functional theory. The current work examines the energetically preferred sites for point defects, such as, Ti vacancy (V_{Ti}), self-interstitials, substitutional and interstitial positions of impurity elements with atomic number 1 (H) through 20 (Ca) as well as several transition metals with atomic numbers larger than that of titanium. The knowledge gained from the current work would eventually help to better understand the diffusion pathways in titanium and would pave way to point defect analysis for commercial alloys such as Ti-6Al-4V.

RESULTS

Titanium in its pure form at room temperature and atmospheric pressure crystallizes in the hcp structure with space group symmetry $P6_3/mmc$ (international space group no. 194). The crystal structure contains two atoms per primitive cell.[32] The lattice parameters as determined from experiments and theoretical studies are shown in Table 1, where the computed values using exchange-correlation functionals such as the local density approximation (LDA[33]) and two different parameterization of generalized gradient approximation (GGA), PW'91[34], and the PBE are compared.

In order to compare the relative stability of different defects, we calculate the formation energy which is derived from the total energies calculated from DFT. The formation energy is given as,[35–37]

$$E_f(\mathrm{D}) = E_{\mathrm{Supercell}}(\mathrm{D}) - E_{\mathrm{Ti-host}} - pn_X\mu_X \quad (1)$$

Here, E_f (D) is the formation energy of a defect D which is measured in the unit of eV/supercell, $E_{\mathrm{Supercell}}$(D) and $E_{\mathrm{Ti-host}}$ are the total energy of the defect and pure supercells, respectively. μ_X is the chemical potential for the species X and n_X is the number of such impurities in the defect supercell. $p = \pm 1$ depending on whether the atom is removed from or added to the host supercell in order to construct the defect supercell. Point defect concentration is proportional to the exponential of formation energy. Formation energy also helps to determine the diffusion coefficient for the kinematics of defects.[38] However, the first principles determination of formation energy calculated from Eq. (1) depends on the choice of μ_X; hence a proper selection of chemical potentials improves the interpretation of the formation energies.

Table 1. Equilibrium lattice parameters of hcp Ti as determined by various exchange-correlation treatments in DFT and their comparison to the experimental values

Method	a (Å)	c (Å)	c/a	References[4]
LDA	2.852	4.523	1.586	Present calc.
PW'91	2.911	4.617	1.586	Present calc.
PBE	2.921	4.633	1.586	Present calc.
Expt.	2.951	4.684	1.587	Ref.[58]
Expt.	2.957	4.685	1.585	Ref. [59]
Expt.	2.949	4.727	1.602	Ref. [60]
Expt.	2.9503 ± 0.004	4.6831 ± 0.004	1.5873	Ref. [61]
Expt.	2.9512 ± 0.002	4.6826 ± 0.002	1.5867	Ref. [61]
Expt.	2.9450	4.6845	1.5907	Ref. [62]
Expt.	2.9504	4.6834	1.5873	Ref. [62]
Expt.	2.951	4.80	1.5859	Ref. [62]
Expt.	2.9503 ± 0.006	4.6810 ± 0.002	1.5866	Ref. [62]
Expt.	2.950	4.681	1.5867	Ref. [62]

In our study, μ_X values are chosen from the pure state of the impurities, called "element" chemical potentials, and the oxides of corresponding impurity elements are called 'oxide' chemical potentials. Details on the sources of μ_X and their role in thermodynamics is presented in the Supporting information.

We note that LDA and GGA fall short in predicting the ground state properties of strongly correlated systems, most notably those of transition metal oxides displaying ferroelectricity, superconductivity, metal-insulator transitions, and magnetism. The problem is more acute for semiconducting properties and magnetic properties and not as severe for simple metallic elements. The situation can ideally be overcome by including an on-site element specific and orbital selective Coulomb repulsion term called the Hubbard U (DFT + U method). However, there is no consensus on using a particular value of U for all the calculations as the values are not transferrable. The actual value of U changes across transition metal elements and their corresponding compounds. This is further complicated by the fact that the value of U is not expected to be same for different crystal structures of the same element or compound. As such, the total energy is dependent on the value of U in the DFT + U method. Since the total energy is the basis of our analysis, we try here avoiding ambiguities that will arise due to including two different levels of theory, DFT and DFT + U and varying the value of U individually for each element.

Self-interstitials

Titanium atoms occupying interstitial lattice sites are self-interstitials. In the hcp crystal lattice, a self-interstitial defect can be located at six sites in the unit cell as shown in Fig. 1.[39] These are called orthogonal (O) and tetrahedral (T) sites. Impurities in basal-tetrahedral (BT) and basal-octahedral (BO) sites lie in the basal plane, midway between two neighboring T sites and O sites along the c direction, respectively. Crowdions are interstitial positions between Ti–Ti bond center and two different configurations have been identified: the basal (CB) and non-basal (CN) crowdions. In contrast to these impurity sites, which can host only one impurity atom per site, dimer-like interstitial point defects comprise two atoms. The two atoms of the dimer-like impurity are symmetrically displaced with respect to a vacant lattice site. Due to the hexagonal symmetry, two orientations exist for the dimer-like point defects. The dumbbell configuration oriented along the c-direction (DC) and the dumb-bell configuration lying in the basal plane (DB) are the unique choices. The DC and DB configurations are split interstitials which are kinds of self-interstitials. The positions of all the eight interstitial configurations are shown in the schematic picture of Fig. 1. The formation energies are summarized for the eight self-interstitial configurations in Ti listed in Table 2. The supercell is comprised of a periodic repetition of hcp primitive lattice units within which the impurity atoms are accommodated. This supercell is geometrically optimized by the conjugate gradient scheme in order to minimize the internal strain. The characteristic impurity positions in the optimized supercell are ascertained by examining its nearest neighbor. The formation energy difference and the total energy difference are identical for isolated self-interstitial defects. However, the formation energy has an advantage as it allows comparison of split interstitial energetics with cases of substitutional and interstitial defect configurations.

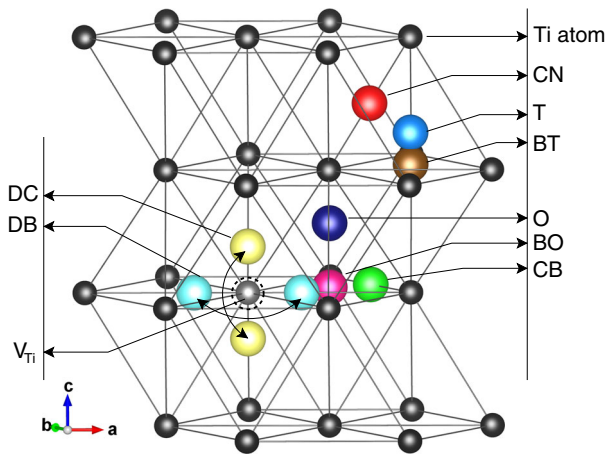

Fig. 1 Schematic crystal structure showing the positions of different type of self-interstitial positions in an hcp Ti lattice. The positions of the tetrahedral (T), orthogonal (O), base tetrahedral (BT), base orthogonal (BO), crowdion in the basal (CB) and non-basal (CN) planes, and the split interstitial along the c-direction (DC) and in the basal plane (DB) are marked. Table 2 lists the relative stability of these defects in Ti host

Table 2. Comparison of E_f (in eV per supercell) for the eight configurations of self-interstitials (shown in Fig. 1)

Index	Start configuration	E_f^U	E_f^R	ΔE_f^{UR}
1	O	6.368	2.168	4.200
2	T	7.406	2.176	5.230
3	T	8.611	3.190	5.421
4	BO	6.053	1.913	4.140
5	CB	11.344	1.911	9.433
6	CN	12.279	2.514	9.765
7	DC	5.016	2.189	2.827
8	DB	5.039	2.084	2.955

The formation energies obtained from the starting and the relaxed models are represented by E_f^U and E_f^R, respectively. $\Delta E_f^{UR}(=E_f^U - E_f^R)$ shows the chemical energy gained. Note that the relaxed configuration of CB is identical to BO, other configurations retained their characteristic positions

The bond length of the spilt interstitial was calculated as 1.663 and 1.930 Å for DC and DB, respectively. The starting geometries were selected by choosing the configuration with lowest total energy after performing a check of total energy as a function of impurity pair bond length in pure lattice. The formation energies are shown in Table 2 for the initial (E_f^U) and relaxed (E_f^R) supercells for various configurations. In other words, E_f^U indicates the energy of impurity interstitial dimers when the host atoms are not relaxed. The difference in the energy ($\Delta E_f^{UR} = E_f^U - E_f^R$) accounts for the gain in the chemical energy at the expense of local lattice distortions. The Ti–Ti bond lengths are 1.430 and 1.463 Å for CN and CB configurations, respectively, which is about half of the equilibrium lattice constant. ΔE_f^{UR} appears large for crowdion self-interstitials; 9.4 and 9.8 eV for CB and CN, respectively, due to the magnitude of E_f^U which is already large owing to additional Ti atom in between Ti–Ti equilibrium bonds. In comparison to this, the energy difference ΔE_f^{UR} is minimal for split interstitial configurations, DC and DB, as the two impurity atoms are positioned in the interstitial region close to their equilibrium separation due to the way the DC and DB models are prepared.

We find that the BO configuration is the most favorable self-interstitial configuration. The energy of the CB configuration is similar to the energy of the BO configuration. The relaxed supercells of the CB configuration are identical to the BO configuration. The results previously reported in ref. [29] that the DB configuration is the most favorable self-interstitial configuration contradicts with our results. In fact, our unrelaxed supercell results match the conclusions of ref. [29] (see column E_f^U in Table 2).

Vacancy-interstitial pairs

The formation energy of an atom missing from a lattice site, i.e., a vacancy (V_{Ti}, not to be confused with vanadium substituted on Ti site, V_{Ti}), is calculated as

$$E_f(V_{Ti}) = E(Ti + V_{Ti}) - \mu_{Ti} \quad (2)$$

where E is the total energy and the value of μ_{Ti} derived from Ti bulk is found to be 1.94 eV, which is similar value to that obtained from ultra-soft pseudopotentials calculations.[40] Energies of Ti vacancies are obtained in a similar range with different exchange-correlation functionals,[41] which are overestimated than that reported in experiment (1.55 eV in ref. [42] and 1.27 eV from positron annihilation spectroscopy in ref.[43]). The discrepancy is due to the lack of density-based exchange correlation to account an accurate electron correlation treatment.[44] There is a way to overcome the limitations of GGA by adding the Hubbard U correction term. However, this was not used in our study because of the ambiguity it introduces in the treatment of chemical potentials which affects the calculation of the formation energies. The energetics shows that the magnitude of vacancy formation energy is comparable to self-interstitials, see Table 2. Thus, it might be assumed that both vacancies and self-interstitials are likely to respond simultaneously to thermodynamic perturbations, which could be coupled to derive a migration mechanism for Ti atom to jump from a lattice position to the nearest interstitial position. The consideration of μ_{Ti} derived from Ti bulk models involve a situation where the vacancy lattice is in thermodynamic equilibrium with perfect bulk Ti. However, this may not be realistic in engineering processes, especially if the displaced Ti atom of interest remains deep in the bulk sample forming secondary phases with other defects/impurities in the lattice. The most trivial case for our discussion would be defect complexes consisting of vacancy and self-interstitial impurity.

In order to obtain insight into defect complexes, we have calculated the formation energy of a V_{Ti}–interstitial Ti pair as a function of the separation of the individual components, i.e., the titanium vacancy, V_{Ti}, and the interstitial titanium atom. Supercell models were prepared with interstitial Ti in the BO configuration and V_{Ti} created at different positions such that the distance of V_{Ti} from the interstitial Ti is 2.15, 4.20, 4.58, 6.44, and 9.23 Å. After minimizing the internal forces in the supercells (geometrical optimization) it is found that for the first three shorter pair separations the interstitial Ti is expected to be attracted to an empty lattice site which may result in elimination of the defect. However, at larger separations of 6.44 and 9.23 Å the interaction between V_{Ti} and the interstitial titanium atom is screened by the host atoms in between. As a result, V_{Ti} and the interstitial Ti atom are trapped into local energy minima without any appreciable change in their separation distance. The formation energies for the three shortest separation distances are identical and are almost 3.9 eV lower in energy than the formation energies of the two larger distances. Ideally, from the energetics it could be expected that vacancies and interstitials should annihilate each other and thus re-establish the environment of an ideal hcp lattice if these defects are in close proximity.

Table 3. Formation energies (in eV per supercell) of impurities at various positions in hcp Ti (refer Fig. 1)

At. no.	Element	O	T	BT	BO	CB	CN	DC	DB	X_{Ti}
1	H	−2.715	−2.617	−2.589	−2.016	−2.596	−1.905	−3.616	−3.943	0.078
3	Li	2.626	2.999	3.577	2.507	2.504	2.748	2.757	2.653	0.752
4	Be	1.358	2.198	3.927	1.517	1.576	1.587	1.152	0.509	−0.197
5	B	3.151	1.769	1.773	1.299	0.773	0.664	−0.066	−0.111	0.522
6	C	−1.703	0.355	0.362	1.496	−0.340	−0.249	1.075	0.283	2.147
7	N	−3.701	−1.998	−1.997	−0.017	−2.261	−2.034	−1.789	−0.026	2.193
8	O	−5.554	−4.370	−4.364	−2.226	−4.368	−3.932	−7.102	−7.247	0.014
9	F	−3.535	−2.902	−2.899	−1.375	−2.915	−2.335	−4.888	−6.140	−0.762
11	Na	4.830	5.026	5.027	5.222	5.219	4.599	5.247	5.304	2.183
12	Mg	3.612	4.062	4.018	4.004	3.240	3.307	4.707	4.425	0.414
13	Al	2.154	3.902	3.386	2.597	1.955	1.889	2.439	1.583	−0.992
14	Si	0.828	1.861	2.879	1.711	0.871	0.760	0.769	−0.089	−1.633
15	P	−1.059	1.335	1.337	0.507	−0.425	−0.613	−0.847	−1.494	−2.005
16	S	−1.861	0.282	0.285	0.373	−0.729	−1.069	−0.168	−1.948	−1.234
17	Cl	−0.369	1.201	1.205	1.940	0.795	0.465	1.796	0.176	0.589
19	K	7.040	6.841	6.844	7.784	6.591	6.896	11.401	10.467	4.488
20	Ca	2.548	3.670	3.207	3.661	2.318	2.392	2.468	3.127	0.166
23	V	1.855	1.897	3.216	1.657	1.652	2.125	1.578	1.678	0.477
28	Ni	1.117	1.219	1.791	1.023	0.886	1.045	0.089	−0.237	−0.369
29	Cu	2.157	2.477	3.054	2.123	2.027	2.056	2.184	2.331	0.026
40	Zr	3.193	3.381	3.384	3.470	3.104	6.165	4.247	7.714	0.191
42	Mo	1.610	2.654	2.658	1.885	1.874	1.690	1.553	1.466	0.091
47	Ag	3.312	3.322	3.969	3.423	2.670	2.744	3.733	3.085	0.186
73	Ta	2.915	2.8721	3.674	3.011	3.002	3.140	3.635	3.505	0.322
74	W	2.794	2.874	3.922	3.119	2.967	2.868	3.718	3.544	0.773
79	Au	2.221	2.190	2.941	2.316	1.564	1.583	1.733	1.028	−0.890
82	Pb	3.997	3.994	4.239	4.459	3.012	3.144	5.244	4.024	0.112

The total energies are taken from optimized geometries. The chemical potentials are taken from elemental compounds (see Supporting information)

Table 4. Formation energies (in eV per supercell) of impurities at various positions in hcp Ti (refer Fig. 1)

At. no.	Element	O	T	BT	BO	CB	CN	DC	DB	X_{Ti}
1	H	0.816	0.913	0.941	1.514	0.934	1.625	3.444	3.117	3.608
3	Li	5.395	5.768	6.346	5.276	5.273	5.517	8.295	8.191	3.521
4	Be	7.240	8.080	8.809	7.398	7.458	7.469	12.916	12.273	5.685
5	B	6.587	5.205	5.209	4.735	4.209	4.100	6.806	6.762	3.959
6	C	2.192	4.251	4.258	5.392	3.555	3.647	8.867	8.074	6.043
7	N	−3.659	−1.956	−1.955	0.025	−2.219	−1.991	−1.704	0.059	2.235
8	O	−1.158	0.026	0.032	2.170	0.028	0.463	1.689	1.544	4.382
9	F	−3.307	−2.674	−2.671	−1.147	−2.687	−2.106	−4.431	−5.684	−0.533
11	Na	6.742	6.938	6.939	7.134	7.131	6.511	9.071	9.128	4.095
12	Mg	9.089	9.539	9.496	9.481	8.718	8.784	15.662	15.381	5.891
13	Al	9.756	10.504	10.987	10.199	9.557	9.491	17.642	16.785	6.609
14	Si	9.259	10.293	11.312	10.142	9.303	9.192	17.632	16.774	6.798
15	P	5.827	8.221	8.224	7.394	6.461	6.273	12.926	12.279	4.882
16	S	1.239	3.383	3.386	3.473	2.371	2.032	6.033	4.253	1.866
17	Cl	−0.692	0.878	0.881	1.617	0.471	0.142	1.149	−0.471	0.265
19	K	8.521	8.322	8.324	9.264	8.072	8.376	14.362	13.428	5.968
20	Ca	7.592	8.714	8.250	8.705	7.362	7.436	12.556	13.215	5.209
23	V	9.532	9.575	10.894	9.335	9.330	9.803	16.934	17.033	8.155
28	Ni	2.236	2.338	2.910	2.142	2.005	2.164	2.327	2.001	0.750
29	Cu	3.352	3.671	4.249	3.317	3.221	3.250	4.573	4.720	1.220
40	Zr	13.368	13.556	13.559	13.645	13.279	16.339	24.597	28.065	10.367
42	Mo	6.804	7.848	7.852	7.079	7.068	6.884	11.942	11.854	5.285
47	Ag	2.958	2.968	3.616	3.070	2.317	2.390	3.026	2.378	0.655
73	Ta	12.875	12.832	13.633	12.971	12.962	13.100	23.555	23.425	10.282
74	W	11.229	11.309	12.357	11.553	11.401	11.302	20.587	20.413	9.208
79	Au	2.460	2.429	3.181	2.555	1.803	1.822	2.211	1.506	−0.650
82	Pb	5.984	5.982	6.226	6.447	4.999	5.131	9.219	7.999	2.099

The total energies are taken from optimized geometries. The chemical potentials are taken from oxide compounds (see Supporting information)

Interstitial and substitutional impurities

Formation energies of the impurities for interstitial and substitutional positions in hcp Ti lattice are calculated from "elemental" chemical potentials ($\mu^{element}$) and 'oxide' chemical potentials (μ^{oxide}), see Supporting information, that are listed in Tables 3 and 4, respectively. For example, Fig. 2a shows the formation energies calculated for O impurity in Ti. The formation energies towards the lower range is obtained from total energy of an O_2 molecule, which could be interpreted as a thermodynamic condition with an oxygen rich environment, while the formation energies towards the upper range is derived from TiO_2 in the rutile structure, which could be interpreted as a thermodynamic condition with oxygen deficient environment. The horizontal dashed lines in this figure denote the configuration with lowest formation energies in each case. It is observed that the O atom favors an octahedral interstitial position when the environment is oxygen deficient. On the other hand, in an environment with rich supply of oxygen the thermodynamic stable phase is oxygen impurity pairs resulting in DB and DC configurations (see Fig. 1). The relative differences in the formation energies of interstitial and substitutional positions for the two types of chemical environment can be estimated from the data of Fig. 2a.

The lower the formation energy of a defect configuration, the higher the probability of finding such a defect in the sample. Fig 2b shows the lowest formation energies obtained for different elements, H (atomic number = 1) through Ca (atomic number = 20), except for noble gas elements He and Ne. Additional selected elements from 3d, 4d, and 5d series transition metal elements, V, Ni, Cu, Zr, Mo, Ag, Ta, W, Au, and Pb, are considered in order to compare the trend of formation energies of elements for relatively larger atomic size. The formation energies of these cases are shown in the shaded region of Fig. 2b. The trend in the lowest formation energies (among the various configurations of impurities) in Fig. 2b which is derived from $\mu^{element}$ is marked by the red line. The formation energies obtained from μ^{oxide} are marked by the blue line in the same figure. It is found that these chemical potential treatments lead to two different trends in the lowest formation energies.

In general, metallic impurities, irrespective of their atomic sizes and exposure to type of chemical environment (consideration of two different chemical potentials), favor the substitutional sites. On the other hand, common highly electronegative elements such as, C, N, O, F, S, and Cl, do not favor the substitutional site. Instead, the elements C, N, and Cl prefer octahedral interstitial sites for the two chemical environments. H, O, and S stabilize different impurity configurations in different chemical potential treatment: octahedral impurity configurations for μ^{oxide} and impurity-dimer (DB and DC) configurations for $\mu^{element}$. Fluorine is the only element which forms impurity-dimer in Ti for both types of chemical potentials. It must be emphasized that H, which could easily lose its electron forming a H^+ cation, actually behaves similarly to the electronegative elements when inserted as an impurity in Ti. This result corroborates the charge transfer analysis where H is observed to acquire electrons from neighboring Ti atoms, which is the discussed in the following section.

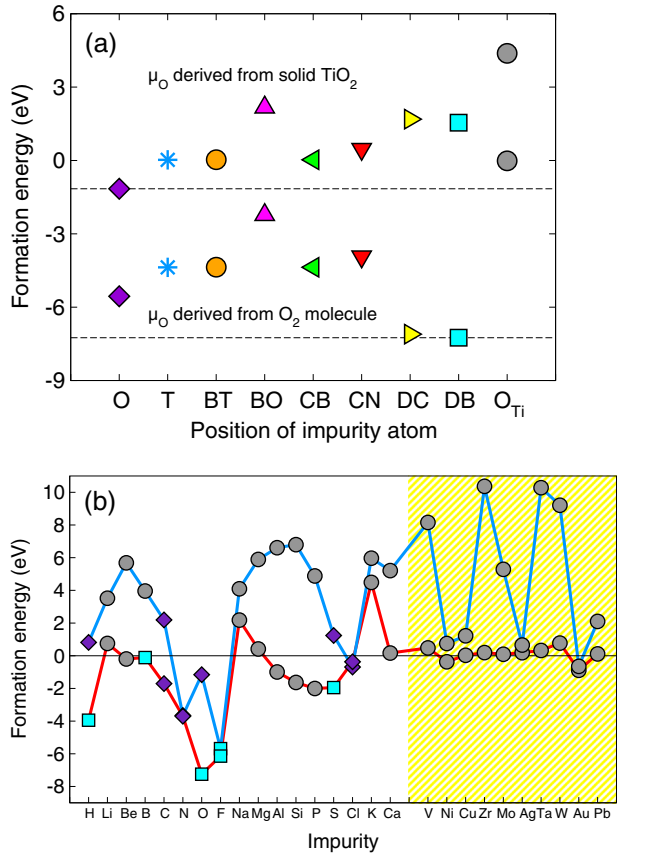

Fig. 2 Comparison of formation energies of impurity elements in various interstitial positions and on the substitutional site. The O impurity is chosen as an example in (**a**). The lower and the upper ranges of formation energies are obtained using μ^{oxide} and $\mu^{element}$ derived from O_2 molecule and TiO_2 solid, respectively, whose values are shown as dashed horizontal lines. **b** Minimum value of formation energies of studied impurities from two sources of chemical potentials. The symbols correspond to the impurity configurations as in (**a**). The data formation energies for selected 3d, 4d, and 5d elements are shown in the shaded (yellow) background

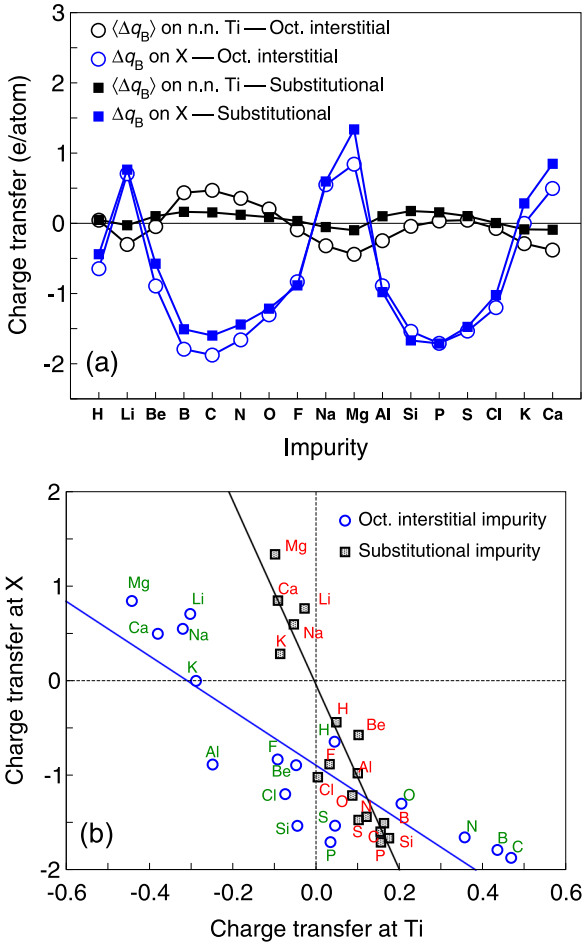

Fig. 3 **a** Charge transfer between the impurity and neighboring Ti atoms. **b** Comparison of the trend in the charge transfer for impurities in octahedral interstitial and substitutional positions

Charge analysis

Chemical hybridization plays an important role for the configuration of impurity atoms in host lattices. An ideal measure of the orbital hybridization strength is the charge transfer between impurity and host atoms. The Bader charge analysis[45,46] provides a quantitative assessment for the accompanied charge transfer.

$$\Delta q_B(\mathrm{X}) = q_B^{\mathrm{reference}}(\mathrm{X}) - q_B^{\mathrm{hybridized}}(\mathrm{X}), \quad (3)$$

where $q_B^{\mathrm{reference}}$ is the integral valence charge supplied in the pseudopotentials of X and $q_B^{\mathrm{hybridized}}$ is the calculated Bader charge after self-consistent field solutions have been achieved. According to this definition, negative values for $\Delta q_B(X)$ would mean charge accumulation from the neighborhood to the atomic site X (the definition is consistent with the definition of electron charge treated as negative), while positive value would mean charge lost from the atomic site X to the surrounding. The tendency of $\Delta q_B(X)$ for impurity and host atoms are expected to be inversely related, as charge lost or gained at the impurity site should be correlated to charge variations in neighboring host atoms. Negative values of Δq_B are a feature common to electronegative impurities such as C, N, O, and F. The charge transfer to the neighboring host Ti ($<\Delta q_B(\mathrm{Ti})>$) is averaged over nearest neighbor coordination 4, 6, and 12 for an impurity atom located in tetrahedral, octahedral, and substitutional impurity sites, respectively.

Charge transfer between the impurity atoms and the nearest neighbor host Ti atoms is shown as a function of atomic number (apart from noble gases) in Fig. 3a for the octahedral- and substitutional impurity sites. The charge transfer follows the same trend of periods in the periodic table for both impurity sites. The average charge transfer to Ti is lower in magnitude because multiple Ti atoms from the neighborhood bond with the impurity atom. The charge transfer to impurity atoms in octahedral interstitial and substitutional sites differs as a function of average charge transfer of Ti as shown in Fig. 3b. The blue and black solid lines are the trend lines for the data of impurities in octahedral interstitial and substitutional positions, respectively. It is observed from Fig. 3b that the charge transfer on an impurity in substitutional cases (slope of the black line) is generally larger than that for octahedral impurity positions (slope of the blue line). The same information is also depicted in Fig. 3a where we mark the difference in charge transfer values between substitutional (filled squares) and interstitial (open circle) cases. As already pointed out in the previous section, H in Ti metal is found to have negative values of Δq_B for both substitutional and interstitial cases (see Fig. 3a,b) suggesting that it acts as an electron attracting impurity, similar to C, O, and F.

The preferred configuration for the considered elements are summarized in Fig. 4, where the formation energies of substitutional impurities is compared with the minimum formation energy of from the interstitial configurations. It is found that highly electronegative elements, H, C, N, O, F, S, and Cl, favor interstitial positions (refer Fig. 2b. The chemical hybridization plays a more

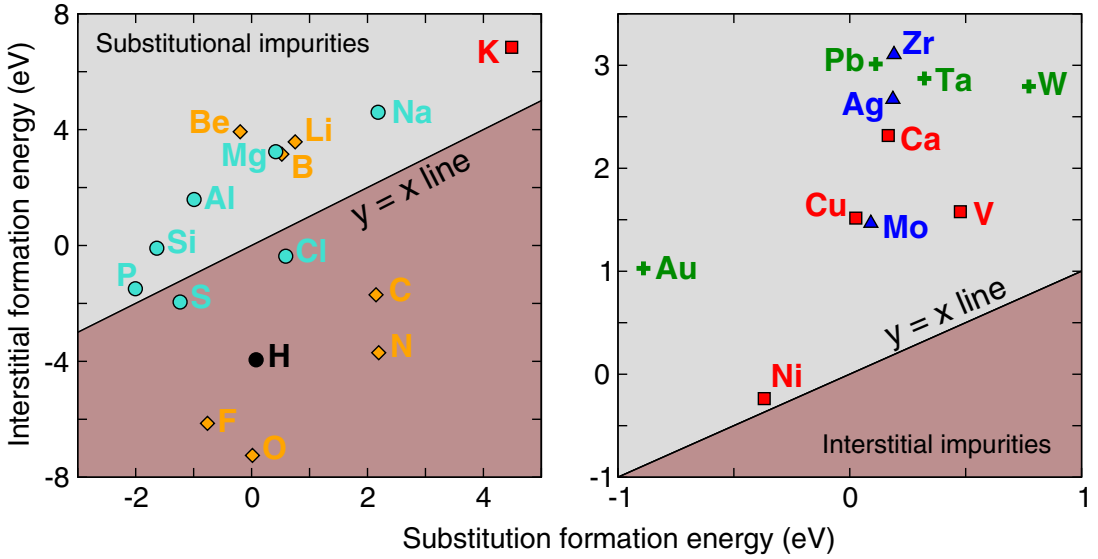

Fig. 4 Comparison of formation energies between the substitutional site (in abscissa) and the most favorable interstitial configuration (in ordinate). The $y = x$ line shows a clear division and suggests the favorable point defect configuration

decisive role than other competing terms. The line $y = x$ is the case where both substitutional and interstitial impurities are equally probable. The farther from this line, the higher the probability of either interstitial or substitutional impurities. The cases of P and Ni impurities deviate from expected behavior. In other words, their formation energies lie relatively close to the $y = x$ line. P is intuitively expected to favor an interstitial position while Ni is expected to favor a substitutional site. Reconsideration of source compounds from which chemical potential is derived could potentially help correct this discrepancy. In addition, for Ni, the difficulty could be in the value of chemical potentials which is derived from the oxide compound NiO. NiO is an example of a compound where the GGA approximation fails to account for the strong electron correlation effects.[47]

DISCUSSION

One of the guiding principles for mixing in metals are the Hume-Rothery rules[48–50] which take in to account: (a) the difference in electronegativity among the involved species, (b) the difference in the size of constituting atoms, (c) electron filling rules (acquiring the octate electronic configuration through hybridization), and (d) the competing crystal structures to explain trends in solid solubility. Similar empirical rules could be formulated for point defect and impurities in metals. Neglecting thermal effects, such guidelines can be derived from the formation energies because they are directly related to the stability of impurities. Although not stated in the original form of the rules, the ionization energy of impurity elements could be included as a descriptor in the present context of point defects, because in order to balance the charges in a single phase system the electronegativity of impurity atoms should be related to the ionization potential of the host atoms and vice versa. The trend in the ionization energy, electronegativity, and the covalent radius of elements are shown in Fig. 5a–f. It is easy to compare the data as a function of the number of valence electrons for the elements in the second (Li through F) and third rows (Na through Cl) of the periodic table and the same as a function of periodic table column number for the elements in fourth, fifth, and sixth rows. The transition metals have multiple potential valence states, which handled by choosing the column number of the periodic table. The value of corresponding physical quantites for Ti is shown as the horizontal dashed line. The lighter elements display distinct trends as compared to the heavier transition elements. With an increase in atomic number, electrons occupy d and f-orbitals appear. These are highly correlated and their chemistry is more involved.

The DFT is a quantitative theory which could provide a way to explain the trends in materials properties, such as those described by the Hume-Rothery rules. Since the formation energies depend on the choice of chemical potential, finding a unique functional dependence of formation energies on physical parameters may not be straightforward. There are further complications for transition metal impurities because of their multi-valence states. The formation energies of corresponding impurities for $\mu^{element}$ and μ^{oxide} for are shown in Figs. 5g, h. The calculations have been performed by allowing volume relaxation of the supercell, which implies that the combined role of electronegativity, ionization potential, covalent radii etc. can be accumulated into one physical descriptor, which is the supercell volume change. The volume change can be captured experimentally by determining the lattice parameters using commonly available characterization techniques, such as the X-ray, electron or neutron diffraction. Figure 6 shows the comparison of volume change for all the impurity configurations. The lowest formation energy configurations are outlined with boxes for each chemical potential treatment (blue for $\mu^{element}$ and green for μ^{oxide}). Please note that for most cases the lowest energy configurations are the same for both chemical potential treatments, hence only the blue box is shown. It is observed that, except for highly electronegative elements of C, N, O, F, S, and Cl, the general trend of lower volume change corresponds to lower formation energies, which is achieved by substitution into the Ti lattice. This is expected because large volume changes in crystal lattice would increase the elastic energy of the system. For comparison, the volume of hcp Ti calculated from DFT is 34.263 Å^3/unit cell, while the bcc Ti is 34.012 Å^3/unit cell (unit cell contains 2 Ti atoms).[51] The difference in volume is 0.251 Å^3/unit cell, which is comparable to the volume change that appears for point defects, especially for transition metal impurities. This is substantial perturbation to the Ti lattice. On the other hand, for highly electronegative elements, the chemical hybridization of point defect with the surrounding host plays a decisive role and these impurities are found in the interstitial position.

Knowledge of positions and formation energies of point defects in Ti and in any base metal are vital. For example, it has been observed that the microstructure of stainless steel is sensitive to the gaseous environment in which the laser melting is

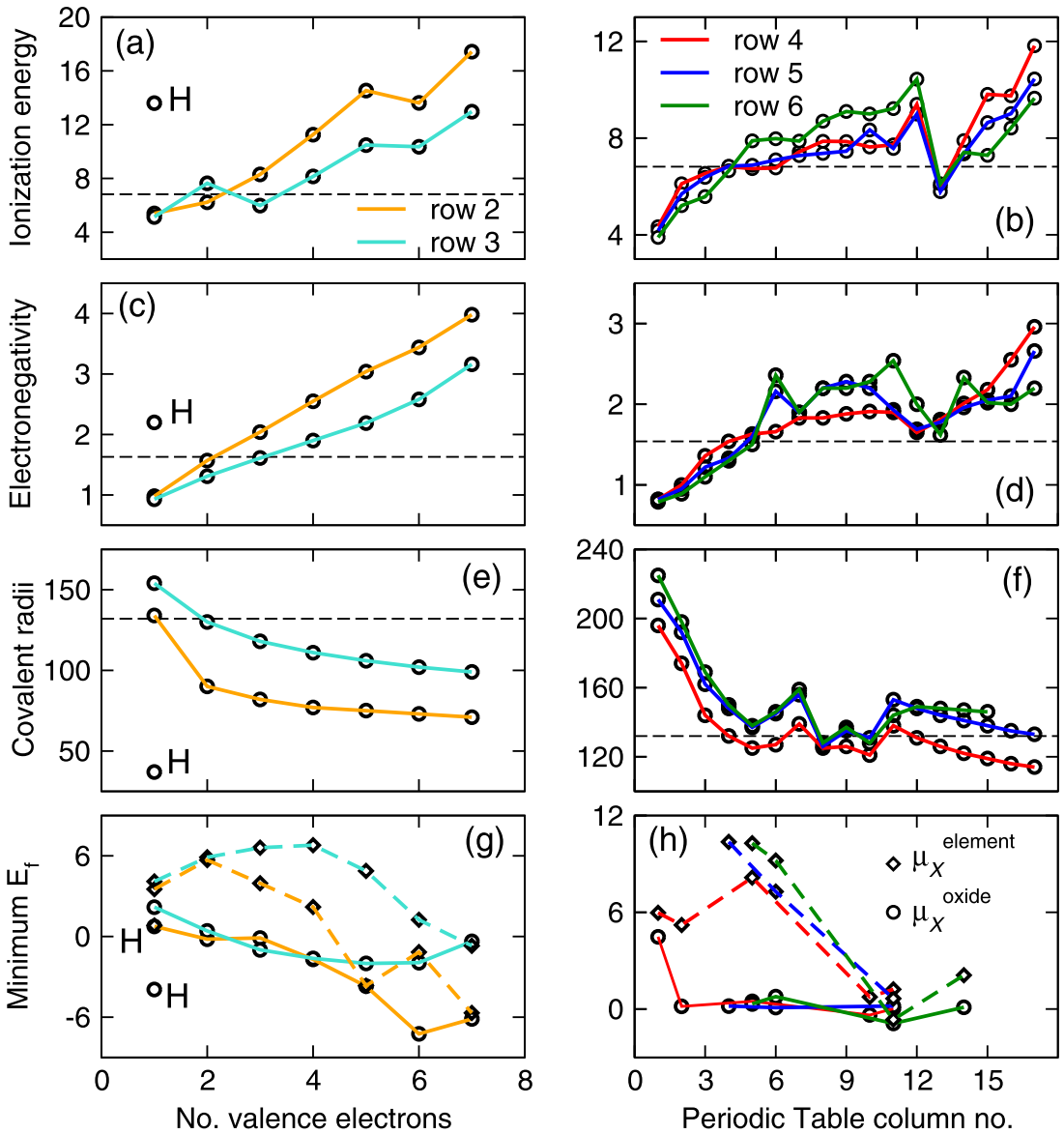

Fig. 5 The trend in the ionization energy, electronegativity and covalent radius of elements as a function of elements as arranged in the periodic table is shown in (**a**–**f**). Note that the data is compared with number of valence electrons for the elements in second (Li through F) and third rows (Na through Cl) of the periodic table and as a function of periodic table column number for the elements in fourth, fifth, and sixth rows, respectively. The value of corresponding physical quantity for Ti is shown as the horizontal dashed line. The lowest formation energies obtained from several configurations are plotted against the abscissa quantities in (**g**) and (**h**), respectively, as the left and right panel plots

performed.[52] Metals are often contaminated by gases during high-temperature processing. Gaseous elements, such as nitrogen in steel, are sometimes deliberately added as an alloying element.[53] Another example; putting together the fact that *c*/*a* ratio of the hcp Ti lattice increases from 1.59 to 1.633 with increasing oxygen content[3,4] and matching the results from Fig. 6 it can be interpreted that O does not favor substitutional or DB interstitial position, to account the positive volume change. Note that the DB (also DC) position is favored at very large oxygen chemical potential surrounding or exposure to very high partial pressure of O_2 gas.

Advancements in processing methods in materials processing, such as laser-based additive manufacturing has led to renewed interest in point defects and their stability due to the fundamental need to control the processing and storage of host powders. The light absorptivity and heating of powders with laser radiation depends on the chemistry together with other factors such as the average particle size distribution and powder surface condition. In order to enhance the degree of absorption, the starting material could be exposed to an appropriate pre-treatment. Doping is one of the methods through which the electronic structure of the starting material could be tuned, for example, to maximize laser absorptivity. A further advantage of laser based additive manufacturing techniques is the potential for controlled processing in different gas environments in a single build allowing for localized microstructure control. Hence, these chemical trends of point defects can lead to the necessary understanding to potentially overcome the challenges of laser absorptivity and phase stability. Thus, despite the fact that thermal effects have been neglected, DFT results provide useful knowledge on the

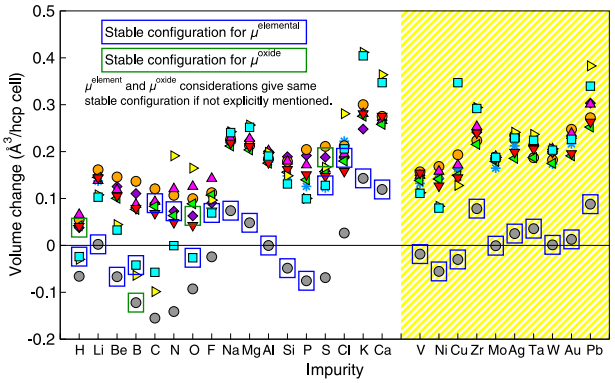

Fig. 6 The change in volume per primitive hcp cell (per two atoms) obtained from the geometrical optimization of the supercell with impurities in various configurations. A positive value of volume change implies tensile hydrostatic strain, while the negative value implies compressive hydrostatic strain. The color code of the impurity configurations is the same as in Fig. 2(a). The lowest formation energy configurations are outlined with blue and green rectangular boxes for $\mu^{element}$ and μ^{oxides}, respectively. Cases for which the lowest energy configurations overlap, only the blue box is shown. The trend that a low volume change is associated with low formation energies is reflected for most impurities, except highly electronegative elements like, C, N, O, F, S, and Cl

physics of point defects and on the materials properties at the ground state.

In conclusion, we have studied the intrinsic and extrinsic point defects in hcp Ti using density functional theory. The impurities are systematically chosen from the periodic table with atomic numbers one through 20 (except the noble gases) and selected elements beyond atomic number 20, such as, V, Ni, Cu, Zr, Mo, Ag, Ta, W, Au, and Pb, in order to understand the trends in the formation of interstitial and substitutional defects. Two chemical conditions represented by elemental chemical potential and oxide chemical potential are explored. The following conclusions are derived from this study:

(i) The base orthogonal (BO) configuration is the energetically most favorable site for self-interstitial Ti atoms in a Ti hcp lattice. The CB (basal crowdion configuration) after geometrical optimization in order to minimize local forces leads to the BO configuration and hence has a similar value of formation energy as the BO configuration.
(ii) Metallic impurities favor substitutional sites in hcp Ti irrespective of their atomic sizes and the chemical environment.
(iii) Highly electronegative elements such as C, N, O, F, S, and Cl have stable configurations at octahedral interstitial positions or as impurity dimers depending on the chemical environment. Although not highly electronegative, hydrogen atoms also energetically favor octahedral interstitial positions. Fluorine is the only element that favors a dimer configuration in hcp Ti for the two chemical conditions studied.
(iv) Defect complexes between vacancies in the hcp Ti lattice and Ti interstitials tend to coalesce and annihilate. They retain their existence only when separated by a distance of more than two lattice parameter units.
(v) We show that the supercell volume change could be good descriptor for the admission of impurities into the Ti lattice. Our results indicate that lower specific volume changes favor more probable impurity configuration due to lower cost in elastic energy. This trend is satisfied by all the transition metal impurities preferring substitutional sites. However, high electronegative elements, such as C, N, O, F, S, and Cl deviate from this trend due to strong chemical hybridization.

METHODS

We used DFT for our theoretical analysis. Spin polarized total energy calculations were performed for a supercell size of $6 \times 6 \times 3$ primitive cells. The supercell has 216 titanium atoms for the pure titanium case. A single point defect in the supercell thus corresponds to a concentration of x~0.46 at% ($Ti_{99.54}X_{0.46}$; $X = V_{Ti}$, elements with atomic number 1 (H) through 20 (Ca) and larger elements, such as V, Ni, Cu, Zr, Mo, Ag, Ta, W, Au, and Pb, roughly scanning element from the 3*d*, 4*d* and 5*d* periods of the periodic table. Impurity dimer cases have x~0.92 at% due to two impurity atoms in the supercell. The GGA is used for the exchange-correlation energy functional as parameterized by Perdew-Burke-Erzernhof[54] together with the projector augmented wave method.[55] The kinetic energy cut-off for the plane waves is set to 500 eV. Integration in the reciprocal space are carried out with the Γ-centered $3 \times 3 \times 3$ *k*-points mesh of the hexagonal Brillouin zone. The supercell was allowed for geometrical optimization with the tolerance criterion for total energy set to 10^{-7} eV in order to minimize the local forces. The DFT calculations were performed using the Vienna ab initio simulation package.[56,57]

Data availability statement

The authors declare that the data supporting the findings of this study are available within the paper and its supplementary information file.

ACKNOWLEDGEMENTS

The financial support from Pratt and Whitney through the UConn—Pratt & Whitney Center of Excellence is gratefully acknowledged. This publication is approved for public release. The computational resources for the work was provided by University Information Technology Services, University of Connecticut.

AUTHOR CONTRIBUTIONS

The study was conceived by S.K.N., C.J.H., S.P.A. and R.J.H. S.K.N. performed the calculations. Results were analyzed with help from all authors. S.K.N., C.J.H., V. S., S.P. A., A.M.D., W.J.B., and R.J.H. contributed to the writing of the manuscript.

ADDITIONAL INFORMATION

Supplementary information accompanies the paper on the *npj Computational Materials* website (https://doi.org/10.1038/s41524-018-0068-9).

Competing interests: The authors declare no competing interests.

Publisher's note: Springer Nature remains neutral with regard to jurisdictional claims in published maps and institutional affiliations.

REFERENCES

1. Smallman, R. E., Harris, J. E. & Society, M. *Vacancies '76: Proceedings of a Conference on"Point Defect Behaviour and Diffusional Processes"', Organized by the Metals Society and Held at the Royal Fort, University of Bristol, on 13–16 September 1976* (Metals Society, 1977).
2. Damask, A. C. & Dienes, G. J. *Point Defects in Metals* (Gordon and Breach, 1963).
3. Fast, N. D. Spanlose Formung von Zirkon und Titan. *Metallwirtsch* **17**, 459–466 (1938).
4. Fischer, E. Thermodynamic calculation of the O-Ti system. *J. Phase Equilib.* **18**, 338–343 (1997).
5. Conrad, H. Effect of interstitial solutes on the strength and ductility of titanium. *Prog. Mater. Sci.* **26**, 123–403 (1981).
6. Simbi, D. J. & Scully, J. C. The effect of residual interstitial elements and iron on mechanical properties of commercially pure titanium. *Mater. Lett.* **26**, 35–39 (1996).
7. Tal-Gutelmacher, E. & Eliezer, D. The hydrogen embrittlement of titanium-based alloys. *JOM* **57**, 46–49 (2005).
8. Jaffee, R. I. & Campbell, I. E. The Effect of oxygen, nitrogen, and hydrogen on iodide refined titanium. *JOM*. **1**, 646–654 (1949).
9. Donachie, M. J. *Titanium and Titanium Alloys*. (American Society for Metals, 1982).
10. Wasz, M. L., Brotzen, F. R., McLellan, R. B. & Griffin, A. J. Effect of oxygen and hydrogen on mechanical properties of commercial purity titanium. *Int. Mater. Rev.* **41**, 1–12 (1996).
11. Donachie, M. J. Jr. *Tiatanium—A Technical Guide* 2nd edn, Vol. 55, 1023–1026 (ASM International, 2000).

12. Lütjering, G. & Williams, J. C. *Titanium*. (Springer-Verlag Berlin Heidelberg, 2007).
13. Hennig, R. G. et al. Impurities block the alpha to omega martensitic transformation in titanium. *Nat. Mater.* **4**, 129–133 (2005).
14. Nishitani, S. R., Kawabe, H. & Aoki, M. First-principles calculations on bcc-hcp transition of titanium. *Mater. Sci. Eng. A* **312**, 77–83 (2001).
15. Ahuja, R., Wills, J. M., Johansson, B. & Eriksson, O. Crystal structures of Ti, Zr, and Hf under compression: theory. *Phys. Rev. B* **48**, 16269–16279 (1993).
16. Yu, Q. et al. Origin of dramatic oxygen solute strengthening effect in titanium. *Science* **347**, 635–639 (2015).
17. Wu, H. H. & Trinkle, D. R. Solute effect on oxygen diffusion in α-titanium. *J. Appl. Phys*. **113** (2013).
18. Wu, X., Wang, R. & Wang, S. Generalized-stacking-fault energy and surface properties for HCP metals: a first-principles study. *Appl. Surf. Sci.* **256**, 3409–3412 (2010).
19. van de Walle, A. & Asta, M. First-principles investigation of perfect and diffuse antiphase boundaries in HCP-based Ti-Al alloys. *Metall. Mater. Trans. A* **33**, 735–741 (2002).
20. Asta, M., De Fontaine, D., Van Schilfgaarde, M., Sluiter, M. & Methfessel, M. First-principles phase-stability study of fcc alloys in the Ti-Al system. *Phys. Rev. B* **46**, 5055–5072 (1992).
21. Huntington, H. B. & Seitz, F. Mechanism for self-diffusion in metallic copper. *Phys. Rev.* **61**, 315–325 (1942).
22. Huntington, H. B. Self-consistent treatment of the vacancy mechanism for metallic diffusion. *Phys. Rev.* **61**, 325–338 (1942).
23. Robrock, K.-H. in *Mechanical Relaxation of Interstitials in Irradiated Metals* (ed. Robrock, K.-H.) 47–75 (Springer Berlin Heidelberg, 1990).
24. Wolverton, C. Solute–vacancy binding in aluminum. *Acta Mater.* **55**, 5867–5872 (2007).
25. Wolverton, C., Ozoliņš, V. & Asta, M. Hydrogen in aluminum: first-principles calculations of structure and thermodynamics. *Phys. Rev. B* **69**, 144109 (2004).
26. Wolverton, C. Crystal structure and stability of complex precipitate phases in Al–Cu–Mg–(Si) and Al–Zn–Mg alloys. *Acta Mater.* **49**, 3129–3142 (2001).
27. Huang, L.-F. et al. From electronic structure to phase diagrams: A bottom-up approach to understand the stability of titanium–transition metal alloys. *Acta Mater.* **113**, 311–319 (2016).
28. Sluiter, M. & Turchi, P. E. A. Phase stability in Ti-V and Ti-Cr alloys: a theoretical investigation. *Phys. Rev. B* **43**, 12251–12266 (1991).
29. Wen, M., Woo, C. H. & Huang, H. Atomistic studies of stress effects on self-interstitial diffusion in α-titanium. *J. Comput. Mater. Des.* **7**, 97–110 (2000).
30. Šob, M., Kratochvíl, J. & Kroupa, F. Theory of strengthening of alpha titanium by interstitial solutes. *Czechoslov. J. Phys. B* **25**, 872–890 (1975).
31. Clouet, E., Caillard, D., Chaari, N., Onimus, F. & Rodney, D. Dislocation locking versus easy glide in titanium and zirconium. *Nat. Mater.* **14**, 931–936 (2015).
32. Partridge, P. G. The crystallography and deformation modes of hexagonal close-packed metals. *Int. Mater. Rev.* **12**, 169–194 (1967).
33. Perdew, J. P. & Zunger, A. Self-interaction correction to density-functional approximations for many-electron systems. *Phys. Rev. B* **23**, 5048–5079 (1981).
34. Perdew, J. P. et al. Atoms, molecules, solids, and surfaces—applications of the generalized gradient approximation for exchange and correlation. *Phys. Rev. B* **46**, 6671–6687 (1992).
35. Baraff, G. A. & Schlüter, M. Electronic structure, total energies, and abundances of the elementary point defects in GaAs. *Phys. Rev. Lett.* **55**, 1327–1330 (1985).
36. Zhang, S. B. & Northrup, J. E. Chemical potential dependence of defect formation energies in GaAs: application to Ga self-diffusion. *Phys. Rev. Lett.* **67**, 2339–2342 (1991).
37. Neugebauer, J. & Van De Walle, C. G. Atomic geometry and electronic structure of native defects in GaN. *Phys. Rev. B* **50**, 8067–8070 (1994).
38. Frank, W., Breier, U., Elsässer, C. & Fähnle, M. First-principles calculations of absolute concentrations and self-diffusion constants of vacancies in lithium. *Phys. Rev. Lett.* **77**, 518–521 (1996).
39. Frank, W. Intrinsic point defects in hexagonal close-packed metals. *J. Nucl. Mater.* **159**, 122–148 (1988).
40. Raji, A. T. et al. Ab initio study of Kr in hcp Ti: diffusion, formation and stability of small Kr-vacancy clusters. *Nucl. Instrum. Methods Phys. Res. B.* **267**, 2991–2994 (2009).
41. Medasani, B., Haranczyk, M., Canning, A. & Asta, M. Vacancy formation energies in metals: a comparison of MetaGGA with LDA and GGA exchange–correlation functionals. *Comput. Mater. Sci.* **101**, 96–107 (2015).
42. Shestopal, V. O. Specific heat and vacancy formation in titanium at high temperatures. *Sov. Phys. Solid State* **7**, 2798–2799 (1966).
43. Hashimoto, E., Smirnov, E. A. & Kino, T. Temperature dependence of the Doppler-broadened lineshape of positron annihilation in α-Ti. *J. Phys. F. Met. Phys.* **14**, L215–L217 (1984).
44. Carling, K. et al. Vacancies in metals: from first-principles calculations to experimental data. *Phys. Rev. Lett.* **85**, 3862–3865 (2000).
45. Tang, W., Sanville, E. & Henkelman, G. A grid-based Bader analysis algorithm without lattice bias. *J. Phys. Condens. Matter* **21**, 84204 (2009).
46. Bader, R. F. W. *Atoms in Molecules: A Quantum Theory*. (Clarendon Press, 1990).
47. Dudarev, S. L., Savrasov, S. Y., Humphreys, C. J. & Sutton, A. P. Electron-energy-loss spectra and the structural stability of nickel oxide: An LSDA+U study. *Phys. Rev. B* **57**, 1505–1509 (1998).
48. Mizutani, U. Hume-Rothery rules for structurally complex alloy phases. *Mrs. Bull.* **37**, 169 (2012).
49. Darken, L. S. & Gurry, R. W. *Physical chemistry of metals*. (McGraw-Hill, 1953).
50. Massalski, T. B. in *Physical Metallurgy*4th edn (eds. Cahn, R. W. & Haasen, P.) 135–204 (North-Holland, 1996).
51. Argaman, U., Eidelstein, E., Levy, O. & Makov, G. Thermodynamic properties of titanium from ab initio calculations. *Mater. Res. Express* **2**, 16505 (2015).
52. Murr, L. E. et al. Microstructures and properties of 17-4 PH stainless steel fabricated by selective laser melting. *J. Mater. Res. Technol.* **1**, 167–177 (2012).
53. Cottrell, A. *An Introduction to Metallurgy* (Institute of Materials, 1995).
54. Perdew, J., Burke, K. & Ernzerhof, M. Generalized gradient approximation made simple. *Phys. Rev. Lett.* **77**, 3865–3868 (1996).
55. Kresse, G. From ultrasoft pseudopotentials to the projector augmented-wave method. *Phys. Rev. B* **59**, 1758–1775 (1999).
56. Kresse, G. & Furthmüller, J. Efficiency of ab-initio total energy calculations for metals and semiconductors using a plane-wave basis set. *Comput. Mater. Sci.* **6**, 15–50 (1996).
57. Kresse, G. & Furthmüller, J. Efficient iterative schemes for ab initio total-energy calculations using a plane-wave basis set. *Phys. Rev. B* **54**, 11169–11186 (1996).
58. Wood, R. M. The lattice constants of high purity alpha titanium. *Proc. Phys. Soc.* **80**, 783–786 (2002).
59. Vohra, Y. K. & Spencer, P. T. Novel γ-phase of titanium metal at megabar pressures. *Phys. Rev. Lett.* **86**, 3068–3071 (2001).
60. Ehrlich, P. Lösungen von Sauerstoff in metallischem Titan. *Z. für Anorg. und Allg. Chem.* **247**, 53–64 (1941).
61. Dechamps, M., Quivy, A., Baur, G. & Lehr, P. Influence of the distribution of the interstitial oxygen atoms on the lattice parameters in dilute H.C.P. titanium-oxygen solid solutions (90–4000 ppm at). *Scr. Metall.* **11**, 941–945 (1977).
62. Chemikerausschuß der GDMB Gesellschaft Deutscher Metallhütten- und Bergleute e. V. *Titan* (Springer-Verlag, 1951).